Journal of Materials Chemistry

Cite this: *J. Mater. Chem.*, 2012, **22**, 24315

www.rsc.org/materials

FEATURE ARTICLE

Open-circuit voltage in organic solar cells

Boyuan Qi and Jizheng Wang*

Received 10th June 2012, Accepted 4th September 2012
DOI: 10.1039/c2jm33719c

Open-circuit voltage (V_{OC}) is the maximum voltage a solar cell can provide to an external circuit, which is derived from the splitting of hole and electron quasi-Fermi levels. In crystalline Si solar cells, the effective density of states at the bottom (top) of the conduction (valence) band is constant, and the quasi-Fermi level can be directly calculated *via* the Fermi–Dirac distribution. However, in organic materials, similar to amorphous Si, disorder induces gap tail states. Relaxation of carriers into these tail states brings the electron quasi-Fermi level down and the hole quasi-Fermi level up, and hence reduces V_{OC}. Furthermore, carrier recombination of various kinds can cause additional loss of V_{OC}. This article reviews the research progress in understanding the origin of V_{OC} in organic solar cells. In particular, the dependence of V_{OC} on four important factors, namely temperature, light intensity, work function of the electrode and material microstructure are discussed based on the model of density of states. Techniques to enhance V_{OC} are also briefly introduced and their mechanisms are analysed.

1 Introduction

The work process of a solar cell has four consecutive steps: (1) the active layer absorbs light and generates excitons; (2) the excitons dissociate into free carriers (holes and electrons); (3) the free carriers drift to their respective electrodes under the force of built-in potential; (4) the free carriers are collected by the electrodes and provide power to the external circuit. If the solar cell is at the open-circuit state, the free carriers generated under steady illumination will accumulate at the anode and cathode, forming a potential difference which cancels out the built-in potential. Under this condition, carrier generation and recombination

Beijing National Laboratory for Molecular Sciences, CAS Key Laboratory of Organic Solids, Institute of Chemistry, Chinese Academy of Sciences, Beijing 100190, China. E-mail: jizheng@iccas.ac.cn

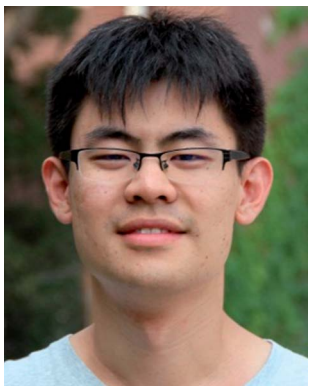

Boyuan Qi

Boyuan Qi received his B. S. degree from the Department of Physics at Nankai University in 2008 and obtained his M. S. degree from the Department of Physics at Peking University in 2011. He is now a Ph.D student at the Institute of Chemistry, Chinese Academy of Sciences. His research interests include device engineering and device physics in organic opto-electronics.

Jizheng Wang

Professor Jizheng Wang got both his B. S. degree (1994) and M. S. degree (1997) from the Department of Physics at Lanzhou University (majored in Semiconductor Device Physics), and earned a Ph.D degree from the Institute of Semiconductors, Chinese Academy of Sciences (2001) in the area of inorganic electronics (III–V quantum dot/well lasers). He worked on organic electronics at Cavendish Laboratory as a post-doc guided by Professor Henning Sirringhaus and Professor Richard H. Friend (2002–2005). After that, he moved to the US in 2005 and worked in the same area at several institutions (Columbia University/Dupont, Arizona State University/US Army Flexible Display Centre). In 2010, he returned to the Chinese Academy of Sciences as a professor, and continues his research in organic electronics at the Institute of Chemistry.

exactly balance each other and no net current exists at any point inside the device. The system is now in a quasi-equilibrium state, and the potential difference formed between the two electrodes is the open-circuit voltage (V_{OC}), which represents the maximum voltage a solar cell can provide to an external circuit.

Many reports have shown that in organic solar cells (OSCs), V_{OC} is linearly related to the difference between the highest occupied molecular orbital (HOMO) level of the donor material and the lowest unoccupied molecular orbital (LUMO) level of the acceptor material, and it does not depend much on the work functions of the electrodes. Maybe the most famous work was done by Brabec *et al.*[1] in 2001. They synthesized a series of fullerene derivatives with different LUMO levels and blended them with a common donor poly(2-methoxy-5-(3′,7′-dimethyloctyloxy)-1,4-phenylenevinylene) (MDMO-PPV). In their experiments, V_{OC} was always linearly dependent on the LUMO level of the acceptor. While the work function of the cathode varied in the wide range of 2.87 eV (Ca) to 4.28 eV (Au), the variation of V_{OC} was comparatively very small (<0.2 V). In 2006, Scharber[2] carefully studied a series of OSC devices (26 polymer donor materials with different HOMO levels blended with a common acceptor), and proposed an empirical equation to express V_{OC}:

$$V_{OC} = (1/q)(|E_{HOMO,D}| - |E_{LUMO,A}| - 0.3\ \text{V}) \quad (1)$$

where q is the elementary charge, $E_{HOMO,D}$ is the HOMO level energy of the donor and $E_{LUMO,A}$ is the LUMO level energy of the acceptor. It should be noted that the V_{OC} loss of 0.3 eV is empirical, and the loss could be greater or smaller. The origin of such a loss has been discussed for a long time.

In general, V_{OC} originates from the splitting of electron and hole quasi-Fermi energy levels triggered by light illumination:

$$V_{OC} = (1/q)(E_{Fn} - E_{Fp}) \quad (2)$$

where E_{Fn} and E_{Fp} are the electron and hole quasi-Fermi levels, respectively. In crystalline Si solar cells (with normal doping and under normal sun light illumination), the electron and hole quasi-Fermi levels are close to the conduction and valence bands, respectively. So V_{OC} in crystalline Si solar cells is approximately equal to the bandgap. However in amorphous Si solar cells, disorder induces gap tail states. The distribution of photogenerated carriers in such gap tail states downshifts the electron quasi-Fermi level and upshifts the hole quasi-Fermi level, which obviously reduces V_{OC}. For the same reason, disorder in organic materials plays a role in bringing the electron quasi-Fermi level down away from the LUMO level of the acceptor, and lifting up the hole quasi-Fermi level away from the HOMO level of the donor, and hence ultimately reducing V_{OC}. In Section 2 of this article we review research progress in understanding such V_{OC} losses based on the model of density of states (DOS), where additional V_{OC} loss induced by carrier recombination is also discussed. In Section 3, four important parameters, namely temperature, light intensity, work function of the electrode and material microstructure, and how they impact V_{OC}, are presented. In Section 4, another model—the charge transfer (CT) state model—of V_{OC} is briefly outlined. In Section 5, the last section of this review, techniques to enhance V_{OC} and their mechanisms are introduced.

2 Origin of V_{OC}

2.1 Equivalent circuit of solar cells

The equivalent circuit of an ideal solar cell is shown in Fig. 1(a), and consists of a constant current source, a diode and an external load. Under illumination a solar cell works like a current source, providing a current density of J_{ph}. A proportion of this current counteracts the junction current of the diode, and the residual current flows to the load. According to Shockley's theory, the junction current density of the diode is presented by:

$$J_d = J_0[\exp(qV/k_BT) - 1] \quad (3)$$

where T is the temperature, k_B is the Boltzmann constant, and J_0 is the reverse saturation current density (in a p–n junction solar cell, J_0 represents the current density of minority carriers, which is a summation of the hole current in the n region and the electron current in the p region). V is the output voltage (generally in a test, we simulate the potential drop on the load with an externally applied voltage to counteract the output voltage of the cell. Therefore V is also the voltage applied during the test).

However, series resistance R_s and shunt resistance R_{sh} have to be taken into account in a practical solar cell,[3] whose equivalent circuit is shown in Fig. 1(b). R_s is composed of the resistance of the bulk active layer, the resistance of electrodes and the contact resistance between the active layer and the electrodes, *etc.* R_{sh} originates from various kinds of current leakage, such as current leakage in the p–n junction, current leakage from the edge of the cell, current leakage induced by impurities in the cell, *etc.* The current density J recorded on the load can be written as:

$$J = \frac{R_{sh}}{R_{sh}+R_s}\left\{J_0\left[\exp\left(\frac{q(V-JR_s)}{mk_BT}\right)-1\right]+\frac{V}{R_{sh}}\right\} - J_{ph} \quad (4)$$

Under the conditions of an open circuit, $V = V_{OC}$, $J = 0$, and with the assumption that $R_{sh} \gg R_s$, V_{OC} can be expressed as:

$$V_{OC} = \frac{mk_BT}{q}\ln\left(\frac{J_{ph}}{J_0}+1\right) \quad (5)$$

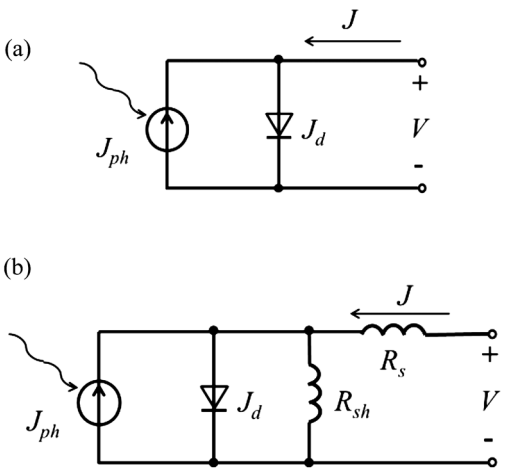

Fig. 1 Equivalent circuit of (a) an ideal solar cell and (b) a practical solar cell.

It is noted that in eqn (4) and (5), a new parameter m is introduced, which is the ideality factor of the diode. It qualifies the property of the diode. In the case of an ideal diode, there is no carrier recombination in the depletion region (*i.e.* no recombination current), diffusion current is dominant in the device, and $m = 1$. In the opposite case, if there is no diffusion current and only recombination current is considered, then $m = 2$. In a practical diode, the current involves both recombination current and diffusion current, so the value of m normally varies in the range of 1 to 2. From eqn (5), V_{OC} is directly proportional to m. It is worth noting here that eqn (5) becomes unreliable if the quality of the diode is too poor ($m > 2$).

In a normal test environment under 1 sun illumination at room temperature ($T = 300$ K), for a given material system the variation in J_{SC} is usually within one order of magnitude ($\sim$10 mA cm^{-2}). In contrast, J_0 is found to be very adjustable (it can vary within several orders of magnitude), and hence it is a crucial parameter that determines V_{OC}. J_0 in OSCs has been extensively studied.

Potscavage *et al.*[4,10] found that J_0 in their pentacene/C_{60} device was exponentially dependent on temperature, and concluded that the dark current comes from the thermally activated injection of carriers at the pentacene–C_{60} interface. Their experimental data can be expressed as:

$$J_0 = J_{00} \exp\left(\frac{-\Phi_B}{k_B T}\right) \quad (6)$$

where J_{00} is a prefactor determined by carrier generation and recombination rate, and Φ_B is the activation energy. Potscavage also proposed that the activation energy can be written as the offset between the HOMO level of the donor and the LUMO level of the acceptor (ΔE_{DA}) divided by a factor (larger than 1), which is used to cover various non-ideal effects such as vacuum level misalignments and the formation of charge transfer states.

Similar to this work, Perez and co-workers[31] also studied J_0 in small molecules/C_{60} based OSCs, and found that J_0 could be expressed as:

$$J_0 = J_{00} \exp\left(\frac{-\Delta E_{DA}}{2mk_B T}\right) \quad (7)$$

Here the factor 2 is introduced by considering the fact that in the process of thermal activation, two free carriers (a hole and an electron) are simultaneously generated at the donor–acceptor interface. Substituting eqn (6) or (7) into (5), the relationship between V_{OC} and ΔE_{DA} can immediately be seen. However, it should be stressed that both these conclusions are reached based on small molecular solar cells, in which the donor–acceptor interface is relatively simple. How far these conclusions can apply to polymer bulk heterojunction (BHJ) solar cells is still under discussion. Another important point that should be noted is that the validity of Shockley's equation (which is derived from inorganic crystal solar cells) in OSCs implies there must be some important fundamental common ground between organic devices and their inorganic counterparts.

2.2 V_{OC} in crystalline and amorphous Si solar cells

In order to gain a better understanding of V_{OC}, it is necessary to review the working principles of crystalline Si p–n junction cells, which form the solid base for almost any solar cells later developed.

Before p-type Si and n-type Si come into contact with each other, they have the same valence band energy (E_V) and conductive band energy (E_C), while their Fermi levels are different due to the different dopant types (the Fermi level of p-type Si is close to E_V, and n-type to E_C, as shown in Fig. 2(a)). When they are brought together, due to the presence of a carrier concentration gradient, the electrons of n-type Si will diffuse to p-type Si, and the holes of p-type Si will diffuse to n-type Si. Redistribution of electrons and holes produces a built-in potential, under which the carriers drift and form a drift current, whose direction is opposite to the diffusion current. When equilibrium is reached, the two currents are equivalent and there is no net current flow inside the junction. The Fermi levels of the two Si semiconductors are now the same, $E_{Fn} = E_{Fp}$. In Fig. 2(b), we can see that all the energy bands of p-type Si are upshifted, and the bands of n-type Si are downshifted. It is clear that $E_C^p - E_C^n = E_V^p - E_V^n = qV_{BI}$ (V_{BI} is the built-in potential under equilibrium), and V_{BI} equals the initial energy difference between E_{Fn} and E_{Fp} (before they come into contact with each other).

When Si is irradiated with light, photogenerated excitons are immediately thermally dissociated into free electrons and holes. They then drift in opposite directions under the force of the built-in potential. The potential of the p side increases and the n side decreases, generating a so-called photo-voltage, which plays a role in cancelling out the built-in potential. Under open circuit conditions, their potentials eventually equal each other, and the system reaches a quasi-equilibrium state. The photo-voltage now is V_{OC}. From Fig. 2(c), it is clear that $qV_{OC} = E_{Fn} - E_{Fp}$.

In amorphous Si solar cells the situation is fundamentally similar to that in crystalline Si devices, but certain modifications should be made to the conduction band and the valence band. As a comparison to the spatially periodic atoms in crystalline Si, the

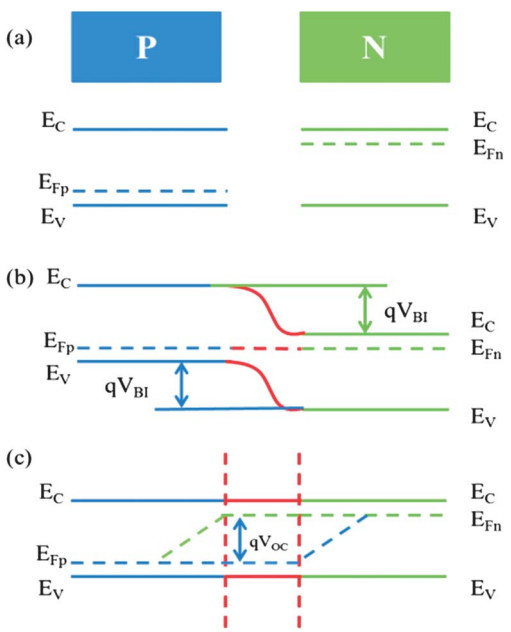

Fig. 2 A Si p–n junction: (a) before contact (b) after contact (c) junction under illumination.

atomic array in amorphous Si is ordered at short range but disordered at long range. Subsequently, the periodic potential in amorphous Si is influenced by the disorder, inducing localized states around the top of valence band and the bottom of conduction band called tail states. Models of bands in crystalline Si and amorphous Si are shown in Fig. 3(a) and (b), respectively. Considering energy disorder in amorphous Si solar cells, the effective bandgap can be given by $E_C - E_V - \Delta$, where Δ is a reduction caused by the disorder-induced tail states around the conduction band and the valence band.

It is easy to understand why tail states can cause a loss in V_{OC}: photogenerated electrons and holes will firstly prefer to occupy tail states rather than the energy states in the conduction band and the valence band, and this lowers the average energy of the electrons and holes, leading to a lower electron quasi-Fermi level and a higher hole quasi-Fermi level.

2.3 V_{OC} in OSCs

Materials for OSCs, especially polymers, are soft materials. In the process of film preparation, kinks in the polymer chains, interactions between molecules, and the degrees of crystallinity of polymers and fullerenes can all introduce disorder into the system. Furthermore, the regioregularity, molecular weight, and purity variation are all important causes of disorder. Control of film growth is now becoming an important subject in the field of OSCs. Thus disorder should also be taken into consideration when discussing origin of V_{OC} in OSCs.

The HOMO and LUMO levels are two important concepts in organic materials. Generally, they refer to the frontier orbitals of a single isolated molecule. However, Ishii *et al.*[67] pointed out that in a polyatomic molecule or a polymer chain, the molecules interact mainly by the weak van der Waals force, and thereby only the upper atomic orbitals (AOs) will merge to form delocalized molecular orbitals (MOs). Deeper AOs are still localized on each atom. The intermolecular band widths introduced by the merging of AOs are less than 0.1 eV. Therefore the terms HOMO level and LUMO level are also widely used in organic solids.

The value of the HOMO level is often determined by means of cyclic voltammetry and photoemission yield spectroscopy, while the value of the LUMO level is usually measured by cyclic voltammetry or calculated by adding up the measured HOMO level and the measured optical bandgap. The DOS declines rapidly as the tail extends deeper into the bandgap, which is eventually beyond the range that the instrument can detect. Therefore the measured value of the HOMO level is usually lower than its actual value, and that of the LUMO level is usually higher than its actual value (the concepts of HOMO level and LUMO level in organic materials are similar to those of valence band and conduction band in inorganic materials). This means that the bandgap we obtain from ΔE_{DA} ($|E_{HOMO,D}| - |E_{LUMO,A}|$) is often larger than the actual effective energy gap, so V_{OC} measured in practical devices is generally lower than ΔE_{DA} obtained from measured HOMO/LUMO levels.

Disorder induced tail states have been reported in several organic materials,[69–71] and the DOS distribution of these tail states can be approximated as a Gaussian or exponential type, with typical widths of 0.1 to 0.2 eV.[72] Here, for simplicity, only the Gaussian model (red dotted lined in Fig. 3(c)) is discussed, as the conclusion reached by the exponential law is similar. Under a Gaussian distribution, DOS can be written as:

$$g_{D/A}(E) = \frac{N_{D/A}}{\sigma\sqrt{2\pi}} \exp\left[-\frac{\left(\pm E \mp E_{HOMO,D/LUMO,A} \right)^2}{2\sigma^2} \right] \quad (8)$$

where E is energy, $N_{D/A}$ represents total density of hole or electron states, and σ characterizes the width of the Gaussian DOS. The effective bandgap of the system can be represented by $\Delta E_{DA} - \sigma^2/k_B T$.[9] It is clear that the broader the DOS (larger σ), the lower the effective energy gap, and hence the lower the V_{OC}.

Blakesley[9] has simulated the influence of disorder on V_{OC}, and found that as the disorder increases (σ increases), V_{OC} drops as expected. Meanwhile, both J_{SC} and FF drop along with V_{OC}. This is explained by disorder induced carrier traps, which decrease the carrier mobility.

An example of different occupancy of the DOS leading to variation in V_{OC} is given by Garcia-Belmonte and co-workers.[24] They compared two fullerene acceptors, [6,6]-phenyl C_{61} butyric acid methyl ester (PCBM) and 4,4′-dihexyloxydiphenylmethano [C_{60}]fullerene (DPM_6) (Fig. 4); these two materials have almost the same LUMO level and similar charge transport capability, but different DOS after blending with P3HT (proved by impedance spectroscopy). The much lower DOS of the gap tail in DPM_6 means a much smaller σ, and hence a higher electron quasi-Fermi level, which leads to higher V_{OC}.

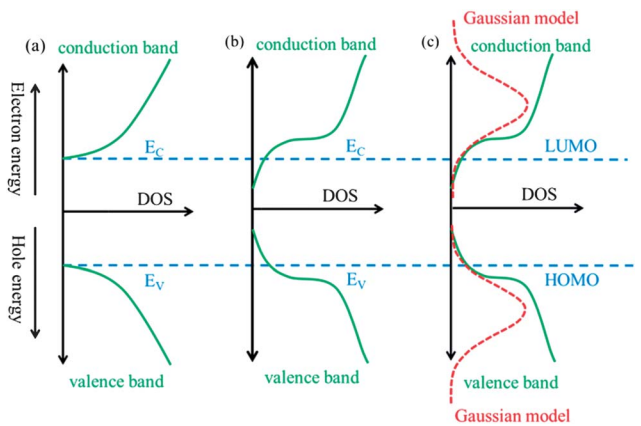

Fig. 3 Models of bands: (a) crystalline Si, (b) amorphous Si and (c) organic material.

2.4 Recombination in solar cells

Shockley and Queisser[41] proposed in 1961 that inevitable radiative recombination sets an upper limit on V_{OC} for all solar cells. Other possible recombination can cause additional loss of V_{OC}, for example, Auger recombination in crystalline Si solar cells, nonradiative recombination in amorphous Si solar cells, and non-geminate recombination in OSCs.[73–75] Recombination, regardless of its type, annihilates carriers and hence causes energy loss, reducing V_{OC} as a result.

In order to quantify the recombination rate R in OSCs, an important question should be clarified: is the recombination monomolecular, or bimolecular, or a combination of the two? In monomolecular recombination, carriers recombine through a

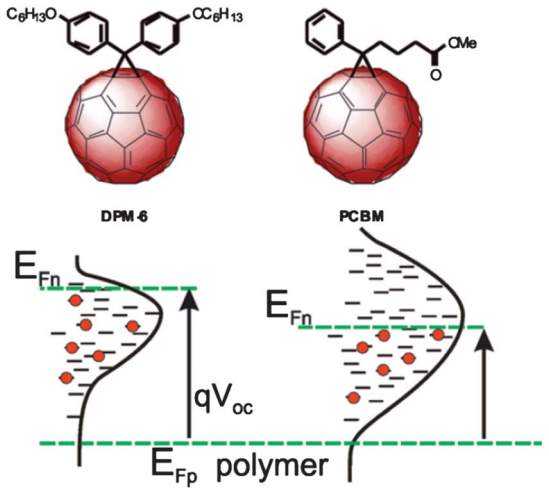

Fig. 4 Molecular structure and DOS scheme of DPM_6 and PCBM. Reprinted with permission from ref. 24. Copyright 2010 American Chemical Society.

trap or a recombination centre, and in the acceptor (donor) material the recombination rate R is proportional to the product of electron (hole) concentration n (p) and electron (hole) trap concentration n_t (p_t), *i.e.*, $R \propto nn_t$ (or $R \propto pp_t$). For bimolecular recombination, $R \propto np$.

A recent study has shown that the recombination mechanism can change from monomolecular at short circuit to bimolecular at open circuit.[49] At short circuit, electrons and holes are spatially separated and swept out quickly by the built-in potential, and the recombination of free electrons and holes is rare, so the dominant recombination is monomolecular (trap-induced). At V_{OC} the built-in potential is cancelled out and photo-generated carriers remain and accumulate inside the device; bimolecular recombination is then greatly increased, which overwhelms the monomolecular recombination.[57] When the cell is connected to an external load, the output photovoltage can vary from 0 to V_{OC} as the resistance of the external load varies from 0 (short-circuit) to ∞ (open-circuit), and the recombination thereby gradually switches from monomolecular dominated to monomolecular/bimolecular co-dominated, and then to bimolecular dominated.

Taking no account of tail states at first and assuming the absorption is the same everywhere in the active layer, the generation rate can be regarded as a constant, G. The bimolecular recombination rate R can be represented by $R(x) = \gamma p(x)n(x)$, where x is the depth in the active layer (the whole thickness of the active layer is L), and γ is the recombination rate coefficient.[9] At open-circuit, $J = 0$, there is no net current, and $G = R(x)$ at any site in the active layer. Blakesley *et al.* applied the Boltzmann approximation, and obtained the expression for $n(x)$ and $p(x)$. Substituting them into $G = R$, V_{OC} can be expressed as:

$$qV_{OC} = \Delta E_{DA} + k_B T \ln\left(\frac{G}{\gamma N_D N_A}\right) \tag{9}$$

If tail states are present, the photogenerated carriers will occupy these tail states *via* the rule of Fermi distribution.[17,26] In case of Gaussian DOS, $n(x)$ and $p(x)$ can be written as:

$$\begin{aligned} n(x,E) &= \int_{-\infty}^{+\infty} g_A(E) f(E) \mathrm{d}E \\ p(x,E) &= \int_{-\infty}^{+\infty} g_D(E)\left[1 - f(E)\right] \mathrm{d}E \end{aligned} \tag{10}$$

Here $f(E)$ is the function of Fermi distribution, and the recombination rate R depends on the conditions of energy state distribution and carrier occupancy. Again using $G = R$, V_{OC} can be expressed:

$$qV_{OC} = \Delta E_{DA} - \frac{\sigma^2}{k_B T} - k_B T \ln\left(\frac{N_A N_D}{np}\right) \tag{11}$$

This is a general expression for V_{OC}. On the right hand side of the equation, there are three terms. The first term is the effective bandgap, ΔE_{DA}, the second term represents disorder-induced V_{OC} loss, and the third term represents carrier recombination induced V_{OC} loss.

3 Important factors related to V_{OC}

There are many factors that can influence V_{OC}. Among them, four are particularly important and the most studied, namely temperature T, illumination intensity P_0, the work function of the electrode, and material microstructure. The dependence of V_{OC} on T, P_0 (impact on n and p) and microstructure (impact on σ) can be immediately seen in eqn (11), while the work function of the electrode determines the contact nature (Ohmic or non-Ohmic), and plays its role *via* surface recombination. In this section, we discuss the effects of the four factors on V_{OC}.

3.1 Temperature

Katz[58] reported that V_{OC} in a BHJ solar cell based on MDMO-PPV:$PC_{61}BM$ decreases linearly when the temperature increases from 10 °C to 60 °C, and attributed this observation to temperature dependent mobility. Similar behaviour was also found in other BHJ systems.[59–61] Linearly fitting the experimental data of V_{OC} *vs.* T under different illumination intensities P_0 has been done by both Cowan[49] and Vandewal[7] for various material systems. They found an interesting phenomenon: all fitting lines for the same material system cross at $T = 0$ K with $V_{OC} = \Delta E_{DA}$. However, detailed experiments on V_{OC} *vs.* T offered different results: for example in the system of $APFO_3$:PCBM, it is found that V_{OC} firstly increases as the temperature decreases, but then saturates at certain temperature, and as the temperature further decreases V_{OC} starts to decrease. Numeral simulations successfully explained such experimental observations.[25,26] Considering the most famous P3HT:PCBM system, ΔE_{DA} is 1 eV (HOMO level of P3HT is 4.9 eV, LUMO level of PCBM is 3.9 eV), $N_D = N_A = 10^{19}$ cm^{-3}, J_{SC} is 10 mA cm^{-2}, σ is 50 meV, the thickness of the active layer (L) is 100 nm, and the recombination coefficient γ is 10^{-12} cm^3 s^{-1}.[49] Under short circuit conditions, J_{SC} approximately equals J_{ph}, and the photocurrent generation rate[76] is simply $G = J_{ph}/eL = J_{SC}/eL$. Using the parameters given above, G is about 6.25×10^{21} cm^{-3} s^{-1}. In case of an open circuit, $G = R = \gamma np$, so $np = G/\gamma = 6.25 \times 10^{33}$ cm^{-6}, and thus the densities of photogenerated holes and electrons are both $\sim 10^{17}$ cm^{-3}. Substituting these values into eqn (11), V_{OC} can be written as: $V_{OC} = 1 - 30/T - 8 \times 10^{-4}\ T$. It is seen there are two

terms related to T. The first term is caused by tail states induced by disorder, with a typical value of 0.1 eV (ref. 9) (the reason that σ is set to 50 meV); the second term is caused by recombination. The concentration of thermally generated carriers (n_i) can be calculated by $G_{\text{therm}} = \gamma N_A N_D \exp(-\Delta E_{DA}/k_B T)$, and $n_i p_i = G_{\text{therm}}/\gamma$, thus $n_i = 2 \times 10^9$ cm^{-3}, which is obviously lower than the concentration of carriers generated by light and can be neglected if the temperature is not very high. So carrier density n and p can be seen as constants in this model. V_{OC} and the two terms related to T are plotted in Fig. 5(a); the grey dashed line is the linear fitting line of V_{OC} *vs.* T, with T at around 300 K (room temperature). It is seen that when T is larger than 200 K, the second term dominates in the equation, and a linear dependence of V_{OC} on T is observed. When T is lower than 200 K, the first term is the main cause of loss, causing deviation of V_{OC} from the linear fit. This can explain why V_{OC} of the $APFO_3$:PCBM device saturates and then decreases at lower T. The phenomenon of V_{OC} saturation can be used to estimate the degree of disorder in OSCs. For a given material system, the density of states (for donor and acceptor materials) can be regarded as constant, and saturation temperature and saturation V_{OC} can both be obtained *via* experiments, thus σ can be calculated based on eqn (11). It is worth noting that based on eqn (11), the lesser the disorder (smaller σ), the lower the saturation temperature, which can be seen in Fig. 5(b).

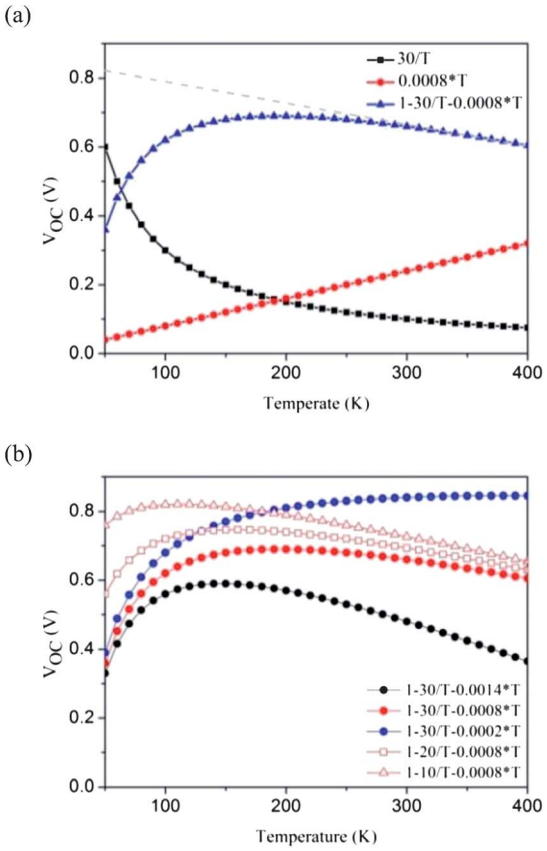

Fig. 5 Linear dependence of V_{OC} on temperature simulated with eqn (11). The grey dashed line in (a) is the linear fitting line of V_{OC} around room temperature.

V_{OC} saturation was also observed by Rand *et al.*[8] in a series of small molecular heterojunction solar cells (Fig. 6). The saturation temperatures of these bilayer solar cells are around 150 K, lower than those observed in BHJ polymer solar cells. This may suggest that disorder is lower in bilayer solar cells than in BHJ cells. In Rand's work, V_{OC} saturation was attributed to the balance between J_{SC} and J_0 (with decreasing the temperature, J_0 declines according to eqn (6), while J_{ph} also decreases due to the decreased electron transfer rate from donor to acceptor. The decrease of J_{ph} should also be partially due to reduced mobility at low temperatures, at which carriers could be seriously localized[81]).

3.2 Light intensity

In Fig. 7(a), the dependence of V_{OC} on light intensity (P_0) can also be seen. The observed logarithmic relationship between V_{OC} and P_0 (ref. 47) can be easily understood based on eqn (11). In this equation, n and p are the only parameters that can be adjusted by P_0. At low light intensity, n and p should change linearly with P_0, resulting in a logarithmic dependence of V_{OC} on P_0. However, when P_0 is large, it will significantly reduce the parallel resistance R_{sh} ($R_{sh} \propto P_0^{-1}$, Rand *et al.*[8,60,77]), and hence the term V/R_{sh} in eqn (4) cannot be neglected anymore, and it plays a role in decreasing V_{OC}, which counteracts the effect of increased n and p. Once the two effects exactly balance each other, V_{OC} will saturate.

3.3 Work function of the electrode

Electrode–active layer contact can also influence V_{OC}. Experiments showed that when the contact deviates too far away from Ohmic, V_{OC} can be largely affected by the cathode work function.[78,79] Such an observation is explained in terms of surface recombination. Under non-Ohmic contact, there is considerable surface recombination at the active layer–cathode interface, whereas under Ohmic contact, such surface recombination is

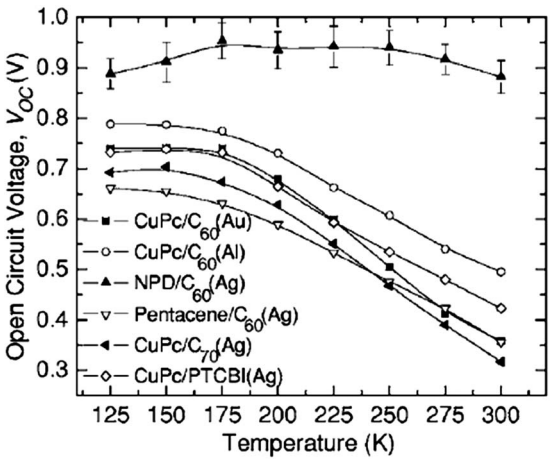

Fig. 6 V_{OC} *versus* T for various donor–acceptor heterojunctions. The metal in parentheses in the legend indicates the cathode material for that device. The error bars displayed for the NPD/C_{60} (Ag) device are typical for all of the heterojunctions. Reprinted with permission from ref. 8. Copyright 2007 American Physical Society.

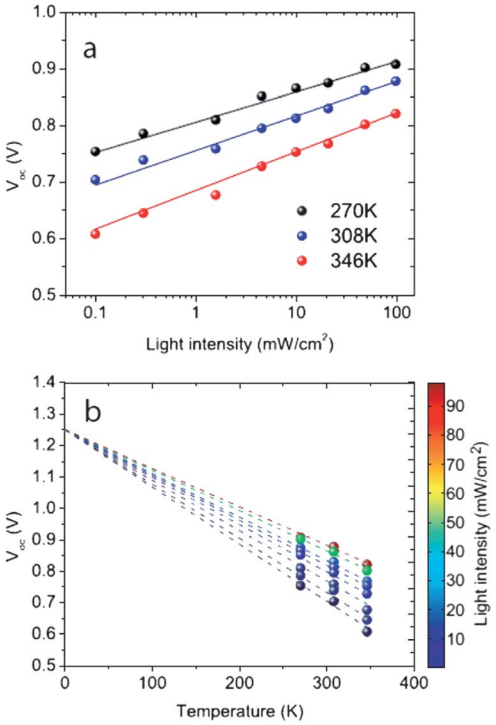

Fig. 7 (a) Logarithmic dependence of V_{OC} on incident light intensity with slope k_BT/e, cell temperature modulated. (b) Linear dependence of V_{OC} on temperature in a PCDTBT:$PC_{71}BM$ solar cell. Reprinted with permission from ref. 49. Copyright 2010 American Physical Society.

greatly suppressed and can hence be neglected (the suppression of surface recombination in Ohmic contact devices and its mechanism for improving V_{OC} have been demonstrated both theoretically and experimentally[55,56]).

If the original Fermi-level of the cathode is higher than the LUMO level of the acceptor, an Ohmic contact can easily be formed *via* electron transfer from the cathode to the acceptor. If the original Fermi-level of the cathode is lower than the LUMO level of the acceptor, electrons can only transfer into the acceptor *via* thermal activation: if the barrier is not very high (<0.2 eV), such transfer is sufficient to form an Ohmic contact, but if the barrier is high, thermal activation cannot generate enough electron transfer, and the contact is non-Ohmic. In case of Ohmic contact, once thermal equilibrium is reached, the Fermi level of the cathode will be levelled and pinned to the LUMO level of the acceptor.[78] The same applies to the donor and anode, where the Fermi level of the anode is pinned to the HOMO level of the donor once an Ohmic contact forms. If the barrier for holes between the anode and the donor is very high, the contact is then non-Ohmic. In a device where both contacts are Ohmic, V_{OC} will be mainly determined by the interfacial kinetics of the donor–acceptor interface,[6] regardless of the work functions of the two electrodes. In other words, V_{OC} is determined by eqn (11). This can explain the experimental observation described in the introduction of this article: only a weak increase of V_{OC} was observed when the cathode of the device (with an active layer of MDMO-PPV blended with PCBM) varied from Al (4.3 eV) to Ca (2.8 eV). When Au acts as the cathode, its original Fermi level (5.1 eV) is much lower than the LUMO level of PCBM (3.9 eV), and thus the contact becomes non-Ohmic. As a result, surface recombination is enhanced and V_{OC} drops accordingly (about 0.1 eV (ref. 1)). If both contacts are non-Ohmic, V_{OC} is then determined by the difference in the work functions of the two electrodes, as predicted by the MIM model (Metal–Insulator–Metal).[54]

V_{OC} is not only influenced by the work function of the electrode,[33] but also by the process by which the electrode is deposited. Metal on organic material, or organic material on metal, can make big difference, because metal on organic material is usually deposited by thermal evaporation at high temperature, and organic material on metal is often deposited by spin-coating or thermal evaporation at low temperature. The former can induce a lot of traps in the active layer by hot metal atoms with high kinetic energies. Hot metal atom induced traps were once an important issue in the P3HT/PCBM system, which can be suppressed by post thermal annealing.

The deposition process of the electrode, the interface between the electrode and the organic material, Fermi-level pinning, and band bending of organic materials can all influence V_{OC}. The detailed effects of these factors can be found in ref. 52, 66–68.

3.4 Material microstructure

Microstructure in BHJ solar cells is difficult to quantify due to the difficulty in accurately measuring the three-dimensional morphology, phase separation, and the interaction between molecules in a working device. Vandewal *et al.*[63] have reported that polymer crystallinity has quite a large effect on blend morphology and V_{OC}. By controlling the thermal treatment temperature for a number of blend films (including P3HT:PCBM), the crystallinity of donor materials and hence the morphology of the blend film can be changed. The energy of charge transfer state (which will be discussed in the next section and is directly related to V_{OC}) is found to vary linearly with the mass fraction of the donor in the form of crystalline nanofibers to the total donor (measured by Fourier-transform photocurrent spectroscopy). Guo and co-workers reported that regioregularity of P3HT can greatly influence charge recombination dynamics at the P3HT–PCBM interface in the blend.[62] The change in recombination dynamics could affect V_{OC}. Therefore controlling the morphology of the BHJ film favourably could be very beneficial to improving V_{OC},[12,29] and researchers have been working extensively to develop such techniques. At present, thermal annealing[23,51] of the blend film and using different solvents to deposit the blend film[21,22,45] are the two most used and most efficient approaches.

Recently, Credgington and Durrant showed that the impact of film microstructure on V_{OC} is determined by detailed recombination dynamics.[100] By the transient photovoltage technique, the recombination rate (and hence lifetime) can be quantified, from which the saturation current density J_0, and hence V_{OC} (substituting J_0 into eqn (5)), can be calculated. For a wide range of tested materials systems, the extracted V_{OC} is very close to the measured one (the average deviation is less than 5 mV). In this way, they successfully related recombination dynamics to the influence of microstructure on V_{OC}.

Meanwhile, Ray *et al.* stated that for a given material system, V_{OC} is determined by the interface area of the bulk

heterojunction (A_{BHJ}).[101] V_{OC} reduces monotonically with increasing A_{BHJ}, *i.e.* there exists an upper limit of V_{OC}^{BHJ} by controlling the morphology. It cannot exceed that of the corresponding planar heterojunction (PHJ) devices, V_{OC}^{PHJ}, because $A_{BHJ} \geq A_{PHJ}$. Therefore, when an as-casted P3HT:PCBM film changes from homogeneous to phase-separated upon thermal annealing, V_{OC} indeed increases. But because the dependence of V_{OC} on A_{BHJ}/A_{PHJ} is logarithmic, even a large value of A_{BHJ}/A_{PHJ} can only result in a slight change of V_{OC}.

In Credgington's review, it is mentioned that the difference in recombination rate for the same material system is very small, while it varies significantly among different systems. This is quite consistent with what Perez and co-workers found in their small molecular OSCs: the molecular composition and the degree of intermolecular interaction can significantly affect the recombination current, and hence V_{OC}.[31] These devices are based on a common acceptor, C_{60}, and a series of donors with different structures (Fig. 8). For example, tetracene and rubrene have similar HOMO levels (5.1 eV for tetracene and 5.3 eV for rubrene), while V_{OC} of the two corresponding devices differs significantly (0.55 V for tetracene and 0.92 V for rubrene). They found that J_0 is the reason for this observation: J_0 of rubrene is about two orders of magnitude lower than that of tetracene, resulting in a higher V_{OC} according to eqn (5). Tetracene is a planar molecule consisting of fused conjugated aromatic rings, while rubrene has four additional phenyl groups connected to the tetracene core perpendicularly. Greater steric hindrance in the structure of rubrene leads to weaker interactions between adjacent rubrene molecules and between the tetracene core and C_{60}, leading to a much lower J_0 (the weaker molecular interactions in rubrene were proved by comparing the spectra of rubrene in solution and in thin film in their experiment).

4 Charge transfer (CT) state

Another prevalent point of view on V_{OC} is that there is a strong relationship between V_{OC} and the emissive CT state.[32,34,38,42] CT state complexes are interfacial electron–hole pairs residing at the donor–acceptor heterointerface, which are also called polaron pairs,[82] charge transfer excitons[64] or exciplexes.[83] Huang *et al.*[65]

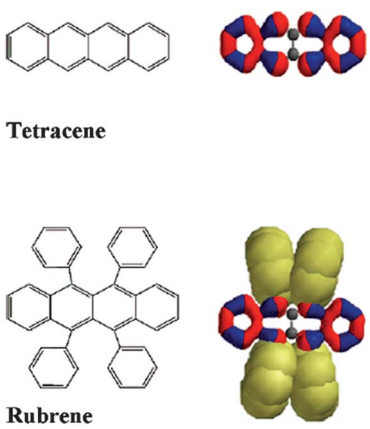

Fig. 8 Molecular structure and electron density distributions of tetracene and rubrene. Reprinted with permission from ref. 31. Copyright 2009 American Chemical Society.

indicated that an exciplex can generally be regarded as a hybrid state with mixed CT and exciton character. The existence of CT states has been proved in a few polymer–fullerene blends and some polymer–polymer blends,[50,84–86] by photo thermal deflection spectroscopy or highly sensitive measurement of the external quantum efficiency spectrum by means of Fourier transform photocurrent spectroscopy. It is demonstrated that CT states can be optically populated by subgap illumination[39,53,87,88] or charge injection (electroluminescence).[89,90]

Due to the low oscillator strength of CT states, only a small fraction of CT states will be occupied under illumination. However, many recent experiments found that the photocurrent and V_{OC} are strongly dependent on CT states,[5,7,53] indicating there are alternative ways to populate them. In a donor–acceptor system, once an exciton photogenerated in the donor material reaches the donor–acceptor interface *via* diffusion, it faces two kinds of energy states: the acceptor singlet state and the CT state. If the energy of the acceptor singlet state is lower than that of the CT state, energy transfer from donor to acceptor will occur. In this case, CT states will not affect V_{OC}. If the energy of CT state is lower, the exciton will populate the CT state, and the newly-formed CT exciton will then either decay to the CT ground state or dissociate into polaron pairs; in this case, CT states will affect V_{OC}.[37]

4.1 Influence of the CT state on V_{OC}

Based on the principle of Detailed Balance, a reciprocity relationship between photovoltaic quantum efficiency and electroluminescent emission was proposed by Rau for p–n junctions:[36,48]

$$\Phi_{EL}(E, V) = EQE_{PV}(E)\Phi_{BB}(E)(\exp(qV/k_BT) - 1) \quad (12)$$

Here, $\Phi_{EL}(E, V)$ is the excess EL intensity, $EQE_{PV}(E)$ is external photovoltaic quantum efficiency, and $\Phi_{BB}(E)$ is the black-body spectrum at 300 K, integrated over all possible incidence angles.

Based on this relationship, the dark saturation current J_0 can be deduced:

$$J_0 = \frac{q}{EQE_{EL}} \int EQE_{PV}(E)\Phi_{BB}(E)\mathrm{d}E \quad (13)$$

EQE_{EL} is the overall EL external quantum efficiency, obtained by integrating $EQE_{EL}(E)$ over all photon energies. V_{OC} can then be directly related to EQE_{EL}, $EQE_{PV}(E)$ and $\Phi_{BB}(E)$ by substituting eqn (13) into eqn (5). This relationship and principle also applies to organic donor–acceptor heterojunctions. After careful mathematical work, the following equation was derived to express V_{OC} for organic donor–acceptor junction cells:

$$V_{OC} = \frac{E_{CT}}{q} + \frac{k_BT}{q}\ln\left(\frac{J_{SC}h^3c^2}{fq2\pi(E_{CT} - \lambda)}\right) + \frac{k_BT}{q}\ln(EQE_{EL}) \quad (14)$$

Here E_{CT} is the free-energy difference between the CT complex ground state and the CT excited state, λ is the reorganization energy associated with the CT absorption process, f is a parameter which is proportional to the density of CT states, h is Planck's constant, and c is the speed of light in a vacuum. At the right hand side of eqn (14), the second and third terms represent V_{OC} loss from non-radiative recombination and radiative

recombination, respectively. Detailed deduction of J_0 and V_{OC} can be found in the paper by Vandewal *et al.*[7] Their experimental results agree quite well with what the model of CT states predicts (eqn (13) and (14)). They also successfully explained the dependence of V_{OC} on temperature T and illumination intensity P_0 based on the model of CT states.

4.2 Relationship between CT and DOS

Both the CT state and the DOS model can sufficiently explain eqn (1). In the CT state model, loss of V_{OC} is attributed to carrier recombination at the donor–acceptor interface *via* CT states (radiative and non-radiative), which increases dark saturation current and causally reduces V_{OC} according to eqn (5). Meanwhile in the DOS model, the loss of V_{OC} is ascribed to gap tail states in donor and acceptor materials. In other words, the CT state model is based on the donor–acceptor interface, while the DOS model is based on bulk donor and acceptor materials. CT states only exist at the donor–acceptor interface, they are formed upon the formation of the interface due to donor–acceptor intermolecular interaction, whereas gap tail states are related to the properties of the material, and they are intrinsically the same across the whole donor (or acceptor) film.

For V_{OC}, in both models the dominant recombination is bimolecular at the donor–acceptor interface. In the DOS model, the bimolecular recombination is mainly *via* electron tail states in the acceptor and hole tail states in the donor, whereas in the CT state model, the bimolecular recombination is directly through CT states at the donor–acceptor interface. Although the CT state model can reasonably explain V_{OC} loss, it has been argued[9] that so far it is unable to explain the super-bimolecular recombination behaviour observed in some BHJ OSCs,[80,91,92] which can be interpreted by the DOS model. Further work is needed to gain a deeper understanding in both models.

5 Ways to improve V_{OC}

Based on a fundamental understanding of the physical mechanisms of V_{OC} we have discussed in the previous sections, there are ways to prevent various V_{OC} losses and hence enhance V_{OC} *via* device engineering for given donor–acceptor combinations.

5.1 Enhancing the built-in potential

As we know, V_{OC} is directly related to the built-in potential of a solar cell, and enlarging the built-in potential can obviously enhance V_{OC}. In OSCs, exciton dissociation is strongly dependent on the electric field at the donor–acceptor interface; for given donor–acceptor junction, the larger the built-in electric field the better to exciton dissociation, and the higher the V_{OC}. In Tada's work, a P3HT/PCBM bilayer device was fabricated through a simple film transfer method.[93] They found that the V_{OC} of the bilayer device could be greatly modified by inserting an aligned dipole monomolecular layer between P3HT and PCBM. Depending on the direction of the dipole moments (either weakening or strengthening the built-in field), V_{OC} could be switched to 0.3 or 0.95 V from 0.5 V of the standard bilayer device. After thermal annealing, the dipole monomolecular layer is destroyed, randomly mixing into the P3HT and PCBM. The effect of the dipole-induced electric field then disappears, and V_{OC} reverts to the standard value of 0.5 V. The concept of using dipole moments is a good method for improving V_{OC} in OSCs.

Yuan *et al.* showed that a large, permanent, internal electric field can be produced by incorporating a ferroelectric polymer layer into the device.[94] The electric field, of the order of 50 V μm^{-1}, potentially induced by the ferroelectric layer is tens of times larger than that achievable by the use of electrodes with different work functions. They showed that ferroelectric layers enhanced the efficiency of several types of organic photovoltaic devices from 1–2% (without ferroelectric layers) to 4–5% (with ferroelectric layers). More research on using dipole layers to enhance V_{OC} can be found in ref. 13, 18–20, 43 and 44.

5.2 Restricting the dark current

As shown in eqn (5), V_{OC} is strongly related to J_{SC}/J_0, so suppressing dark saturation current density J_0 is an important strategy to enhance V_{OC}. An electron blocking layer between the active layer and the anode can effectively weaken surface recombination at the anode–active layer interface, and a hole blocking layer between the active layer and the cathode can effectively weaken surface recombination at the cathode–active layer interface. Dark current can thus be significantly suppressed due to reduced surface recombination. Li[40] *et al.* demonstrated in their tin(II) phthalocyanine (SnPc)/C_{60} bilayer device, that dark saturation current density J_0 was reduced by over two orders of magnitude by inserting electron blocking layers (either organic or inorganic); as a result V_{OC} was increased to 0.4 V from the original value of 0.16 V. A series of materials with deep HOMO levels were reported to act as hole (or exciton) blocking materials[27,28,30,95–97] to suppress dark saturation current density J_0 (and/or increase short circuit current density J_{SC}). It is worth noting here that buffer layers with different functions are widely used in OSCs, and the electron and hole blocking layers mentioned here are among them. Buffer layers generally refer to the interfacial layers between active layers and electrodes,[14–16,35,46] which are mainly used to perform the following functions: (1) minimize the energy barrier between the active layer and the electrode, (2) form a selective contact for electrons (holes),[11] and (3) prevent electrode atoms from reacting with the active layer or diffusing into the active layer. The use of buffer layers in OSCs has been elaborated in Yang and Brabec's reviews.[98,99]

6 Conclusions

In OSCs, V_{OC} is generally reported to scale linearly with the difference between the HOMO level of the donor material and the LUMO level of the acceptor material, and a loss of about 0.3 V is often found in practice. In this paper, research progress on the origin of such observations is reviewed. Based on the model of DOS, such V_{OC} loss comes from two sources: disorder-induced gap tail states in the donor and acceptor materials, and bimolecular recombination at the donor–acceptor interface. The linear dependence of V_{OC} on temperature, the logarithmic dependence of V_{OC} on illumination intensity, and the effects of the work function of the electrode as well as material microstructure are summarized and fully discussed in this review. In addition, another important model—the CT state model, which

is grounded on charge-transfer states at the donor–acceptor interface—is briefly introduced. At the end of the review, we outlined techniques used to enhance V_{OC} in OSCs for given donor–acceptor junction cells; these techniques can either strengthen the built-in electric field or suppress dark saturation current, and hence improve V_{OC}. This review attempts to give a brief but comprehensive summary on understanding the behaviour of V_{OC} in OSCs.

Acknowledgements

The authors acknowledge the financial support from the National Natural Science Foundation of China (grant no. 61072014 and 21021091), 973 Program (grant no. 2011CB932304) and Hundred-Talent Program of Chinese Academy of Sciences.

Notes and references

1 C. J. Brabec, A. Cravino, D. Meissner, N. S. Sariciftci, T. Fromherz, M. T. Rispens, L. Sanchez and J. C. Hummelen, *Adv. Funct. Mater.*, 2001, **11**, 374.
2 M. C. Scharber, D. Mühlbacher, M. Koppe, P. Denk, C. Waldauf, A. J. Heeger and C. J. Brabec, *Adv. Mater.*, 2006, **18**, 789.
3 C. Waldauf, M. C. Scharber, P. Schilinsky, J. A. Hauch and C. J. Brabec, *J. Appl. Phys.*, 2006, **99**, 104503.
4 W. J. Potscavage, Jr, S. Yoo and B. Kippelen, *Appl. Phys. Lett.*, 2008, **93**, 193308.
5 K. Vandewal, K. Tvingstedt, A. Gadisa, O. Inganäs and J. V. Manca, *Nat. Mater.*, 2009, **8**, 904.
6 D. Cheyns, J. Poortmans, P. Heremans, C. Deibel, S. Verlaak, B. P. Rand and J. Genoe, *Phys. Rev. B: Condens. Matter Mater. Phys.*, 2008, **77**, 165332.
7 K. Vandewal, K. Tvingstedt, A. Gadisa, O. Inganäs and J. V. Manca, *Phys. Rev. B: Condens. Matter Mater. Phys.*, 2010, **81**, 125204.
8 B. P. Rand, D. P. Burk and S. R. Forrest, *Phys. Rev. B: Condens. Matter Mater. Phys.*, 2007, **75**, 115327.
9 J. C. Blakesley and D. Neher, *Phys. Rev. B: Condens. Matter Mater. Phys.*, 2011, **84**, 075210.
10 W. J. Potscavage, Jr, A. Sharma and B. Kippelen, *Acc. Chem. Res.*, 2009, **42**, 1758.
11 W. Tress, K. Leo and M. Riede, *Adv. Funct. Mater.*, 2011, **21**, 2140.
12 D. Credgington, R. Hamilton, P. Atienzar, J. Nelson and J. R. Durrant, *Adv. Funct. Mater.*, 2011, **21**, 2744.
13 Z. He, C. Zhong, X. Huang, W.-Y. Wong, H. Wu, L. Chen, S. Su and Y. Cao, *Adv. Mater.*, 2011, **23**, 4636.
14 J. Huang, J. Yu, Z. Guan and Y. Jiang, *Appl. Phys. Lett.*, 2010, **97**, 143301.
15 C. Kulshreshtha, J. W. Choi, J.-K. Kim, W. S. Jeon, M. C. Suh, Y. Park and J. H. Kwon, *Appl. Phys. Lett.*, 2011, **99**, 023308.
16 J. Huang, J. Yu, W. Wang and Y. Jiang, *Appl. Phys. Lett.*, 2011, **98**, 023301.
17 G. Garcia-Belmote and J. Bisquert, *Appl. Phys. Lett.*, 2010, **96**, 113301.
18 C.-T. Chou, C.-H. Lin, M.-H. Wu, T.-W. Cheng, J.-H. Lee, C.-H. J. Liu, Y. Tai, S. Chattopadhyay, J.-K. Wang, K.-H. Chen and L.-C. Chen, *J. Appl. Phys.*, 2011, **110**, 083104.
19 C. He, C. Zhong, H. Wu, R. Yang, W. Yang, F. Huang, G. C. Bazan and Y. Cao, *J. Mater. Chem.*, 2010, **20**, 2617.
20 S. O. Jeon, J.-H. Kim, J. W. Kim, Y. Park and J. Y. Lee, *J. Phys. Chem.*, 2011, **115**, 18789.
21 P. P. Boix, M. M. Wienk, R. A. J. Janssen and G. Garcia-Belmonte, *J. Phys. Chem.*, 2011, **115**, 15075.
22 D. M. Stevens, J. C. Speros, M. A. Hillmyer and C. D. Frisbie, *J. Phys. Chem. C*, 2011, **115**, 20806.
23 J. B. Kim, Z.-L. Guan, A. L. Shu, A. Kahn and Y.-L. Loo, *Langmuir*, 2011, **27**, 11265.
24 G. Garcia-Belmonte, P. P. Boix, J. Bisquert, M. Lenes, H. J. Bolink, A. L. Rosa, S. Filippone and N. Martín, *J. Phys. Chem. Lett.*, 2010, **1**, 2566.
25 A. K. Thakur, G. Wantz, G. Garcia-Belmonte, J. Bisquert and L. Hirsch, *Sol. Energy Mater. Sol. Cells*, 2011, **95**, 2131.
26 G. Garcia-Belmonte, *Sol. Energy Mater. Sol. Cells*, 2010, **94**, 2166.
27 B. P. Rand, J. Li, J. Xue, R. J. Holmes, M. E. Thompson and S. R. Forrest, *Adv. Mater.*, 2005, **17**, 2714.
28 B. E. Lassiter, G. Wei, S. Wang, J. D. Zimmerman, V. V. Diev, M. E. Thompson and S. R. Forrest, *Appl. Phys. Lett.*, 2011, **98**, 243307.
29 C. W. Schlenker and M. E. Thompson, *Chem. Commun.*, 2011, **47**, 3702.
30 K. L. Mutolo, E. I. Mayo, B. P. Rand, S. R. Forrest and M. E. Thompson, *J. Am. Chem. Soc.*, 2006, **128**, 8108.
31 M. D. Perez, C. Borek, S. R. Forrest and M. E. Thompson, *J. Am. Chem. Soc.*, 2009, **131**, 9281.
32 J. J. Benson-Smith, L. Goris, K. Vandewal, K. Haenen, J. V. Manca, D. Vanderzande, D. D. C. Bradley and J. Nelson, *Adv. Funct. Mater.*, 2007, **17**, 451.
33 F. Zhang, M. Ceder and O. Inganäs, *Adv. Mater.*, 2007, **19**, 1835.
34 D. Veldman, S. C. J. Meskers and R. A. J. Janssen, *Adv. Funct. Mater.*, 2009, **19**, 1939.
35 H.-L. Yip, S. K. Hau, N. S. Baek, H. Ma and A. K.-Y. Jen, *Adv. Mater.*, 2008, **20**, 2376.
36 T. Kirchartz and U. Rau, *Phys. Status Solidi A*, 2008, **205**, 2737.
37 C. Deibel, T. Strobel and V. Dyakonov, *Adv. Mater.*, 2010, **22**, 4097.
38 A. Maurano, R. Hamilton, C. G. Shuttle, A. M. Ballantyne, J. Nelson, B. O'Regan, W. Zhang, I. McCulloch, H. Azimi, M. Morana, C. J. Brabec and J. R. Durrant, *Adv. Mater.*, 2010, **22**, 4987.
39 L. Goris, A. Poruba, L. Hod'ákova, M. Vaněček, K. Haenen, M. Nesládek, P. Wangner, D. Vanderzande, L. D. Schepper and J. V. Manca, *Appl. Phys. Lett.*, 2006, **88**, 052113.
40 N. Li, B. E. Lassiter, R. R. Lunt, G. Wei and S. R. Forrest, *Appl. Phys. Lett.*, 2009, **94**, 023307.
41 W. Shockley and H. J. Queisser, *J. Appl. Phys.*, 1961, **32**, 510.
42 J. C. Blakesley and N. C. Greenham, *J. Appl. Phys.*, 2009, **106**, 034507.
43 J. Luo, H. Wu, C. He, A. Li, W. Yang and Y. Cao, *Appl. Phys. Lett.*, 2009, **95**, 043301.
44 Z. T. Liu, M. F. Lo, H. B. Wang, T. W. Ng, V. A. L. Roy, C. S. Lee and S. T. Lee, *Appl. Phys. Lett.*, 2009, **95**, 093307.
45 M.-S. Su, C.-Y. Kuo, M.-C. Yuan, U.-S. Jeng, C.-J. Su and K.-H. Wei, *Adv. Mater.*, 2011, **23**, 3315.
46 V. Shrotriya, G. Li, Y. Yao, C.-W. Chu and Y. Yang, *Appl. Phys. Lett.*, 2006, **88**, 073508.
47 C. M. Ramsdale, J. A. Barker, A. C. Arias, J. D. MacKenzie, R. H. Friend and N. C. Greenham, *J. Appl. Phys.*, 2002, **92**, 4266.
48 U. Rau, *Phys. Rev. B: Condens. Matter Mater. Phys.*, 2007, **76**, 085303.
49 S. R. Cowan, A. Roy and A. J. Heeger, *Phys. Rev. B: Condens. Matter Mater. Phys.*, 2010, **82**, 245207.
50 H. Ohkita, S. Cook, Y. Astuti, W. Duffy, S. Tierney, W. Zhang, M. Heeney, I. McCulloch, J. Nelson, D. D. C. Bradley and J. R. Durrant, *J. Am. Chem. Soc.*, 2008, **130**, 3030.
51 F. Padinger, R. S. Rittberger and N. S. Sariciftci, *Adv. Funct. Mater.*, 2003, **13**, 85.
52 J. Hwang, A. Wan and A. Kahn, *Mater. Sci. Eng., R*, 2009, **64**, 1.
53 K. Vandewal, A. Gadisa, W. D. Oosterbaan, S. Bertho, F. Banishoeib, I. V. Severen, L. Lutsen, T. J. Cleij, D. Vanderzande and J. V. Manca, *Adv. Funct. Mater.*, 2008, **18**, 2064.
54 P. W. M. Blom, V. D. Mihailetchi, L. J. A. Koster and D. E. Markov, *Adv. Mater.*, 2007, **19**, 1551.
55 I. Lange, J. C. Blakesley, J. Frisch, A. Vollmer, N. Koch and D. Neher, *Phys. Rev. Lett.*, 2011, **106**, 216402.
56 H. Bässler, *Polym. Adv. Technol.*, 1998, **9**, 402.
57 C. G. Shuttle, A. Maurano, R. Hamilton, B. O'Regan, J. C. de Mello and J. R. Durrant, *Appl. Phys. Lett.*, 2008, **93**, 183501.
58 E. A. Katz, D. Faiman, S. M. Tuladhar, J. M. Kroon, M. M. Wienk, T. Fromherz, F. Padinger, C. J. Brabec and N. S. Sariciftci, *J. Appl. Phys.*, 2001, **90**, 5343.
59 D. Chirvase, Z. Chiguvare, M. Knipper, J. Parisi, V. Dyakonov and J. C. Hummelen, *J. Appl. Phys.*, 2003, **93**, 3376.

60 I. Riedel, J. Parisi, V. Dyakonov, L. Lutsen, D. Vanderzande and J. C. Hummelen, *Adv. Funct. Mater.*, 2004, **14**, 38.
61 M. Kemerink, J. M. Kramer, H. H. P. Gommans and R. A. J. Janssen, *Appl. Phys. Lett.*, 2006, **88**, 192108.
62 J. Guo, H. Ohkita, H. Benten and S. Ito, *J. Am. Chem. Soc.*, 2010, **132**, 6154.
63 K. Vandewal, W. D. Oosterbaan, S. Bertho, V. Vrindts, A. Gadisa, L. Lutsen, D. Vanderzande and J. V. Manca, *Appl. Phys. Lett.*, 2009, **95**, 123303.
64 D. Veldman, Ö. İpek, S. C. J. Meskers, J. Sweelssen, M. M. Koetse, S. C. Veenstra, J. M. Kroon, S. S. van Bavel, J. Loos and R. A. J. Janssen, *J. Am. Chem. Soc.*, 2008, **130**, 7721.
65 Y. Huang, S. Westenhoff, I. Avilov, P. Sreearunothai, J. M. Hodgkiss, C. Deleener, R. H. Friend and D. Beljonne, *Nat. Mater.*, 2008, **7**, 483.
66 P. Kumar, S. C. Jain, H. Kumar, S. Chand and V. Kumar, *Appl. Phys. Lett.*, 2009, **94**, 183505.
67 H. Ishii, K. Sugiyama, E. Ito and K. Seki, *Adv. Mater.*, 1999, **11**, 605.
68 S. Braun, W. R. Salaneck and M. Fahlman, *Adv. Mater.*, 2009, **21**, 1450.
69 T. Sueyoshi, H. Fukagawa, M. Ono, S. Kera and N. Ueno, *Appl. Phys. Lett.*, 2009, **95**, 183303.
70 O. Tal, Y. Rosenwaks, Y. Preezant, N. Tessler, D. K. Chan and A. Kahn, *Phys. Rev. Lett.*, 2005, **95**, 256405.
71 I. N. Hulea, H. B. Brom, A. J. Houtepen, D. Vanmaekelbergh, J. J. Kelly and E. A. Meulenkamp, *Phys. Rev. Lett.*, 2004, **93**, 166601.
72 K. Celebi, P. J. Jadhav, K. M. Milaninia, M. Bora and M. A. Baldo, *Appl. Phys. Lett.*, 2008, **93**, 083308.
73 L. J. A. Koster, E. C. P. Smits, V. D. Mihailetchi and P. W. M. Blom, *Phys. Rev. B: Condens. Matter Mater. Phys.*, 2005, **72**, 085205.
74 C. Groves and N. C. Greenham, *Phys. Rev. B: Condens. Matter Mater. Phys.*, 2008, **78**, 155205.
75 C. G. Shuttle, B. O'Regan, A. M. Ballantyne, J. Nelson, D. D. C. Bradley and J. R. Durrant, *Phys. Rev. B: Condens. Matter Mater. Phys.*, 2008, **78**, 113201.
76 A. M. Goodman and A. Rose, *J. Appl. Phys.*, 1971, **42**, 2823.
77 S. Yoo, B. Domercq and B. Kippelen, *J. Appl. Phys.*, 2005, **97**, 103706.
78 V. D. Mihailetchi, P. W. M. Blom, J. C. Hummelen and M. T. Rispens, *J. Appl. Phys.*, 2003, **94**, 6849.
79 C. J. Brabec, A. Cravino, D. Meissner, N. S. Sariciftci, T. Fromherz, M. T. Rispens, L. Sanchez and J. C. Hummeln, *Adv. Funct. Mater.*, 2001, **11**, 374.
80 C. G. Shuttle, B. O'Regan, A. M. Ballantyne, J. Nelson, D. D. C. Bradley, J. de Mello and J. R. Durrant, *Appl. Phys. Lett.*, 2008, **92**, 093311.
81 V. D. Mihailetchi, J. K. J. van Duren, P. W. M. Blom, J. C. Hummelen, R. A. J. Janssen, J. M. Kroon, M. T. Rispens, W. J. H. Verhees and M. M. Wienk, *Adv. Funct. Mater.*, 2003, **13**, 43.
82 V. Dyakonov and E. Frankevich, *Chem. Phys.*, 1998, **227**, 203.
83 A. C. Morteani, P. Sreearunothai, L. M. Herz, R. H. Friend and C. Silva, *Phys. Rev. Lett.*, 2004, **92**, 247402.
84 M. A. Loi, S. Toffanin, M. Muccini, M. Forster, U. Scherf and M. Scharber, *Adv. Funct. Mater.*, 2007, **17**, 2111.
85 T. Offermans, P. A. van Hal, S. C. J. Meskers, M. M. Koetse and R. A. J. Janssen, *Phys. Rev. B: Condens. Matter Mater. Phys.*, 2005, **72**, 045213.
86 Y. Zhou, K. Tvingstedt, F. Zhang, C. Du, W.-X. Ni, M. R. Andersson and O. Inganäs, *Adv. Funct. Mater.*, 2009, **19**, 3293.
87 T. Drori, C.-X. Sheng, A. Ndobe, S. Singh, J. Holt and Z. V. Vardeny, *Phys. Rev. Lett.*, 2008, **101**, 037401.
88 K. Vandewal, L. Goris, I. Haeldermans, M. Nesladek, K. Haenen, P. Wagner and J. V. Manca, *Thin Solid Films*, 2008, **516**, 7135.
89 H. Kim, J. Y. Kim, S. H. Park, K. Lee, Y. Jin, J. Kim and H. Suh, *Appl. Phys. Lett.*, 2005, **86**, 183502.
90 M. Yamada, T. Akasaka, S. Nagase, K. Tvingstedt, K. Vandewal, A. Gadisa, F. Zhang, J. Manca and O. Inganäs, *J. Am. Chem. Soc.*, 2009, **131**, 11819.
91 G. Garcia-Belmonte, P. P. Boix, J. Bisquert, M. Sessolo and H. J. Bolink, *Sol. Energy Mater. Sol. Cells*, 2010, **94**, 366.
92 G. Juska, K. Genevicius, N. Nekrasas, G. Sliauzys and G. Dennler, *Appl. Phys. Lett.*, 2008, **93**, 143303.
93 A. Tada, Y. Geng, Q. Wei, K. Hashimoto and K. Tajima, *Nat. Mater.*, 2011, **10**, 450.
94 Y. Yuan, T. J. Reece, P. Sharma, S. Poddar, S. Ducharme, A. Gruverman, Y. Yang and J. Huang, *Nat. Mater.*, 2011, **10**, 296.
95 H. R. Wu, Q. L. Song, M. L. Wang, F. Y. Li, H. Yang, Y. Wu, C. H. Huang, X. M. Ding and X. Y. Hou, *Thin Solid Films*, 2007, **515**, 8050.
96 P. Peumans, V. Bulovic and S. R. Forrest, *Appl. Phys. Lett.*, 2000, **76**, 2650.
97 Q. L. Song, F. Y. Li, H. Yang, H. R. Wu, X. Z. Wang, W. Zhou, J. M. Zhao, X. M. Ding, C. H. Huang and X. Y. Hou, *Chem. Phys. Lett.*, 2005, **416**, 42.
98 R. Steim, F. R. Kogler and C. J. Brabec, *J. Mater. Chem.*, 2010, **20**, 2499.
99 L.-M. Chen, Z. Xu, Z. Hong and Y. Yang, *J. Mater. Chem.*, 2010, **20**, 2575.
100 D. Credgington and J. R. Durrant, *J. Phys. Chem. Lett.*, 2012, **3**, 1465.
101 B. Ray, M. S. Lundstrom and M. A. Alam, *Appl. Phys. Lett.*, 2012, **100**, 013307.